CHAPTER FOUR

Methylene blue-eluting nanofibers for antimicrobial photodynamic therapy (APDT) of infected wounds in immunocompromized rats

1. Introduction

Wound infections are a significant health burden worldwide. Infections predispose wounds to a prolonged inflammatory condition which may contribute to delayed healing, morbidity and mortality [377, 378]. Furthermore, the poor health-related quality of life [379, 380] and loss of productivity associated with lengthy wound treatment processes and duration of hospital stay pose a major threat to public health and the economy [381].

Treatment of acute and chronic wounds is highly dependent on the local wound condition, the patient's general health and on the use of the adequate wound healing products [382]. The formulation of wound care products is generally based on antimicrobial agents and wound healing materials. Currently, antibiotics for topical or systemic administration or a combination thereof and as a wide range of wound dressing materials are used in the management of bacterial wound infections [137, 383, 384]. However, bacterial resistance to these antibiotics and emergence of antibiotic-resistant bacteria including methicillin-resistant S. aureus (MRSA), reported world-wide, hampered effective treatment [385, 386]. MRSA is a major cause of hospital-acquired infection throughout the world and is now also prevalent in the community as well as residential homes [387, 388]. Indeed, bacterial resistance urged a need to focus research efforts on maximization of the efficiency of wound care techniques and products as components of an integrated approach based on the best practice guidelines [382, 389].

In the quest for alternative antimicrobial strategies with different mechanisms of action, antimicrobial photodynamic therapy (APDT) has been revived as an effective antimicrobial therapeutic modality not associated with bacterial resistance [390]. The mechanism of action of APDT depends on a potent microbicidal effect in the presence of a non-toxic organic photosensitizer (PS) and light of a specific wavelength [162]. Interaction of these agents with molecular oxygen present in tissue produces cytotoxic singlet oxygen and free radicals which kill the target cells [391]. These reactive oxygen species cause nonspecific damage to cellular components, and therefore it is highly unlikely for bacteria to develop resistance [195]. Only cells able to bind the photosensitizer and receive light efficiently are affected by PDT. Thus, photosensitizers with molecular properties, either inherent or engineered, promoting fast interaction with bacterial cells, will allow preferential inactivation of bacterial cells in comparison to the host cells such as keratinocytes [192]. Compared to existing antimicrobial therapies, APDT provides significant advantages as it is equally effective to kill multi-drug resistant microbes as naïve strains, acts remarkably faster against microorganisms and inactivate bacterial virulence factors [162, 390, 392]. The treatment is restricted to the light-irradiated region and therefore reduces the risk of adverse systemic effects.

As the field of PDT research is dominated mainly by basic scientists and clinicians, clinical advances in PDT have been based on the development of photosensitizers and light sources with improved properties [393, 394]. Little attention has been paid to a rational approach for the effective presentation of photosensitizers, a formulation development component that can impede the translation of PDT research to clinical practice [395]. For current antimicrobial PDT studies, pharmaceutical vehicles used are simple systems, mainly aqueous solutions or oil-in-water creams, gels and patches selected at random as the main aim of these studies was to maximize the bacterial killing effect. Preparation of fresh PS solutions and other dosage forms in the clinical setting and inability of many of these simple vehicles to keep the PS in place at the target site in an effective concentration for a sufficient period of time impeded wider spread clinical use of APDT. Rational development of more effective

complex delivery systems allowing easy administration and effective use of PSs will promote clinical applicability of APDT [395, 396].

Apart from the antimicrobial photosensitizer component, the wound dressing plays an equally important role in the APDT wound repair applications. A wide range of passive, interactive, and bioactive wound care materials with different degrees of clinical merits and limitations have been in use [137, 384]. Biodegradable polymer nanofibers evolved over the last decade as a porous scaffold for tissue engineering and wound healing applications [138, 257]. In wound repair, biodegradable nanofibrous membranes act as a temporary replacement of the native extracellular matrix (ECM) and potential carrier system for the temporally controlled localized delivery of antibacterial agents [46, 257] and wound healing enhancers such growth factors [6]. The large surface area of the nanofibers mesh results in efficient drug release by mass transfer [22], a process that can be modulated by controlling physicochemical characteristics of the polymer membrane [106, 397]. Moreover, nanofibers promote wound microbial cleanliness by restricting bacterial invasion via the sieve effect. By virtue of their structural features, nanofibers inherently promote the hemostasis phase of wound healing and initiate tissue repair by facilitating cell attachment and proliferation [138, 398]. They reduce wound scarring by guiding cell growth [138].

Intuitively, combining photodynamic activation as antimicrobial technique with antimicrobial / photosensitizer eluting nanofibers as a medicated wound healing product provides a multifunctional wound repair approach with greater potentials in the treatment of infected wounds. To this end, two approaches with different mechanisms of action, PS-nanofiber-bacteria interactions and formulation requirements could be envisioned. The first approach involves immobilization of a hydrophobic non-leachable PS onto polymer nanofibers with bacterial eradication depending on the transport of the light-generated singlet oxygen within the fibers matrix to bacteria adhering to the NFs surface. Although the approach proved effective in water disinfection [399], surface disinfection and in the development of implantable biomaterials [400, 401], a single study explored the potential of photoactive textiles in the setting of chronic wound healing [227]. The second approach involves encapsulation of a water-soluble antimicrobial PS into polymer NFs which act as a PS delivery wound healing dressing or scaffold with light-activated bacterial inactivation depending on the binding of the released PS to the target bacterial cells prior to irradiation. For the formulation of NFs as a PS delivery system, the aim should be to modulate the PS release characteristics to allow the delivery of a sufficient amount of the PS within a relatively short period of time for early instant eradication of bacteria, not subjecting the PS to molecular aggregation and maintenance of bacterial wound cleanliness post illumination by the temporally controlled release of PS. This is consistent with a biphasic release profile of PS. Accordingly, the NF matrix by acting as a reservoir for localized PS release may promote both early fast PS release for irradiation and a prolonged dark antimicrobial effect. Provided that the PS dose, light fluence and pre-illumination incubation period are optimized, mixing of the PS with wound fluids, a factor of importance in efficiently inactivating wound bacteria [402], allows achievement of the treatment goal. Other formulation considerations include preservation of the PS photochemical and antimicrobial activity during fabrication of NFs by electrospinning and maximization of the concentration drive for diffusion and equilibrium partitioning between the wound site and NFs matrix.

Regarding PS selection for PS release-based NFs as a wound healing biomaterial, water soluble PS such MB is a good choice. MB has photochemical characteristics conferring to this molecule a great potential for application in PDT [188]. Because of its cationic nature, MB

may double the targeting effect of light towards bacteria by preferential binding to bacterial cells compared to eukaryotic human cells. Although both bacterial and mammalian cells carry a negative charge because of the phosphate groups in phospholipids, the residual negative charge on bacterial surfaces is denser due to negatively charged molecules such as peptidoglycans, lipoteichoic acid, and lipopolysaccharide [191]. In addition, bacteria show greater susceptibility for photosensitization because of their larger size and different structure [192]. MB is active against Gram positive and Gram negative bacteria commonly infecting wounds including resistant strains [374, 403]. Moreover, the ability of MB to mix with wound fluids would promote inactivation of bacteria distributed in the wound bed [200].

In Chapter 1 and chapter 3 of the thesis, MB-loaded electrospun PHB/PEG NFs were developed and characterized for physichochemical attributes including MB release pattern, photophysical and antimicrobial activity both in the dark and upon illumination with a LED at 650 nm. Conditions for efficient bacterial inactivation including light dose, MB concentration and dark incubation time were optimized. The objective of the present study was to investigate the potentials of these NFs as a component of a dual NFs / photoactivation modality for the treatment of infected full thickness excision wounds, in terms of infection management and wound healing promotion, in an immunocompromized rat model. To the best of our knowledge, this is the first *in vivo* study using PS-eluting nanofibers in wound healing applications. Conducting the study at the preclinical level will allow examination of diverse variables involved in the *in vivo* PS-scaffold-bacteria interaction, particularly in the challenging setting of immunocompromized host. Morphological follow-up of the wound healing progress was substantiated with microbiological, histopathological and molecular biology data.

2. Materials and Methods

2.1. Materials

Nanofibers

Plain and MB-loaded nanofibers prepared by emulsion electrospinning of a 15% chloroformic solution of a polymer blend consisting of PHB and PEG 4000 (3: 2) were developed and characterized for pharmaceutical attributes and microbiological activity in Chapter 1 of the thesis. Their photophysical properties were investigated in Chapter 3.

Chemicals

- Sandimmune Neoral® (cyclosporine A, Novartis) soft gelatin capsules, 100 mg
- Thiopental® (Thiopentone sodium injection)Sandoz, Germany
- Savlon® (cetrimide-chlorhexidine solution), Novartis, Egypt.
- TRI reagent (Sigma, St. Louis, MO, USA)
- Reverse Transcriptase, DNase I (Invitrogen, Carlsbad, CA, USA)
- Omniscript Reverse Transcriptase (Qiagen, Valencia, CA, USA)
- Oligo-dT primer (Amersham Pharmacia, Piscataway, NJ, USA)

Culture media

Nutrient Agar, Nutrient Broth and Mannitol Salt Agar (Oxoid Ltd; Basingostok; Hampshire, England) were used.

Microorganism

A standard strain of *Staphylococcus aureus* ATCC 6538P (Sa_{st}) was obtained from the Department of Pharmaceutical Microbiology, Faculty of Pharmacy, Alexandria University. Sa_{st} was maintained and subcultured as described in Chapter 1. The CFU/ml of the final inoculum was checked using the viable count technique whenever necessary and was equivalent to about 10^8 CFU/ml. This inoculum was further diluted as required.

Animals

The experimental animals used were young female *Wistar* rats of 3 month-age and weighing (150 ± 20 g). Rats were obtained from the animal house of the Faculty of Pharmacy, Alexandria University. The rats were kept on a diet providing the daily needs of nutrients and water. The rats were housed individually in cages. They were maintained in a temperature and humidity controlled environment at the animal house of the Faculty of Pharmacy, Alexandria University.

All animal procedures were adopted in accordance with the Guidelines for Ethical Conduct in the Care and Use of Research Animals developed by the American Psychological

Association (APA) Committee on Animal Research and Ethics (CARE). Human care of all animals was strictly followed throughout the *in vivo* study.

2.2. Equipment

- Electrospinning apparatus equipped with High Voltage DC Power Supply (P3508, Raymax, Canada) and a syringe pump (101, KD scientific, USA).
- Vortex mixer (VM-300, KK, USA)
- Adventurer sensitive electrical digital balance (Ohause Corp. Pine Brook, NJ, USA).
- Hot plate magnetic stirrer (IP 21, IKA, Staufen, Germany)
- Micrometer (IP 65, Mitutoyo Manufacturing, Tokyo, Japan)
- Digital camera, 12 mega pixels, 5X optical zoom (ES70, Samsung Co, South Korea).
- Programmable LED power supply with 24 lamp (assembled in-house)
- Light microscope with digital camera (CX41, Olympus America Inc, USA).
- Incubator (BST 5020, MLW, Germany)
- Portable autoclaves (A. Gallenkamp & Co. Ltd, United Kingdom).
- Micropipettes (Comecta, Spain).

2.3. Methods

Antimicrobial photodynamic therapy of infected circular excision wounds in immunocompromized rats

2.3.1. Customization of MB-eluting NFs as dressings for the circular excision wounds

Circular samples of NFs (10 mm diameter, weighing approximately 12 mg and containing MB 60 µg /12 mg membrane) were used for excision wounds. Digital photographs of the dressings customized for the wounds are shown in Figure 58

Figure 58: Digital photograph of the circular MB-loaded nanofibrous sheet used for the treatment of circular excision wounds

2.3.2. The Light source

Photoactivation was performed by using a light emitting diode at 650 nm at a suitable distance from the wound in order to have a light spot corresponding to a diameter of 1.7 cm. The light intensity was 150 mW. A single light dose range of 100 to 200 J/ cm^2, demonstrated

in Chapter 3 to be sufficient for antibacterial effectiveness, was used. The maximum wavelength of MB (660 nm) overlapped with the LED emission of 650 nm.

2.3.3. Pre-operational care techniques

Disinfection and hair clipping:

The surgical table and the operating board were disinfected with Savlon®, (cetrimide-chlorhexidine solution) diluted 1 in 10. Disinfection was performed prior to each surgery. The surgical instruments were sterilized by boiling for 15 minutes in Savlon® solution diluted 1 in 10. The surgical instruments were left to cool for 15 minutes in the dilute Savlon® solution. The antiseptic solution was washed away using 70% alcohol. A new set of surgical instruments was used for each animal.

Anesthesia and hair clipping:

Following a previously reported procedure [404, 405], the rat was weighed and anesthetized with thiopentone sodium (50 mg/kg body weight) administered by intra-peritoneal injection. The dorsal and lateral areas of the animal were clipped with a pair of scissors (other than those used in the surgery). The skin was prepared by scrubbing with dilute solution of Savlon® (1:30). The solution was then washed with sterile normal saline and the skin scrubbed with 70% ethanol. The hair clipping and skin disinfection were performed away from the surgery table, and the animal was transferred to the sterilized surgery table

2.3.4. Surgical procedure and generation of circular S. aureus-infected excision wounds

The rat was stretched prone (lying face down) on the operating board so that the inferior angles of the scapulae, the vertebral column and the hip joints were easily palpated and noticed. Two full skin thickness circular excision wounds of initial average diameter of 12.5 mm were generated on the shaved back of each rat using a pair of scissors, the 2 excisions were just above the hip joints (Figure 59). Excisions were parallel to the vertebral column. All freshly created wounds were washed with normal sterile saline and tapped dry with disposable sterile cotton pads.

All excisions were infected by careful instillation of an inoculum of 50 µl of Sa_{st} (~10^6 CFU/ml) using a micropipette. At 30 min after infection, the wounds were subjected to different treatments.

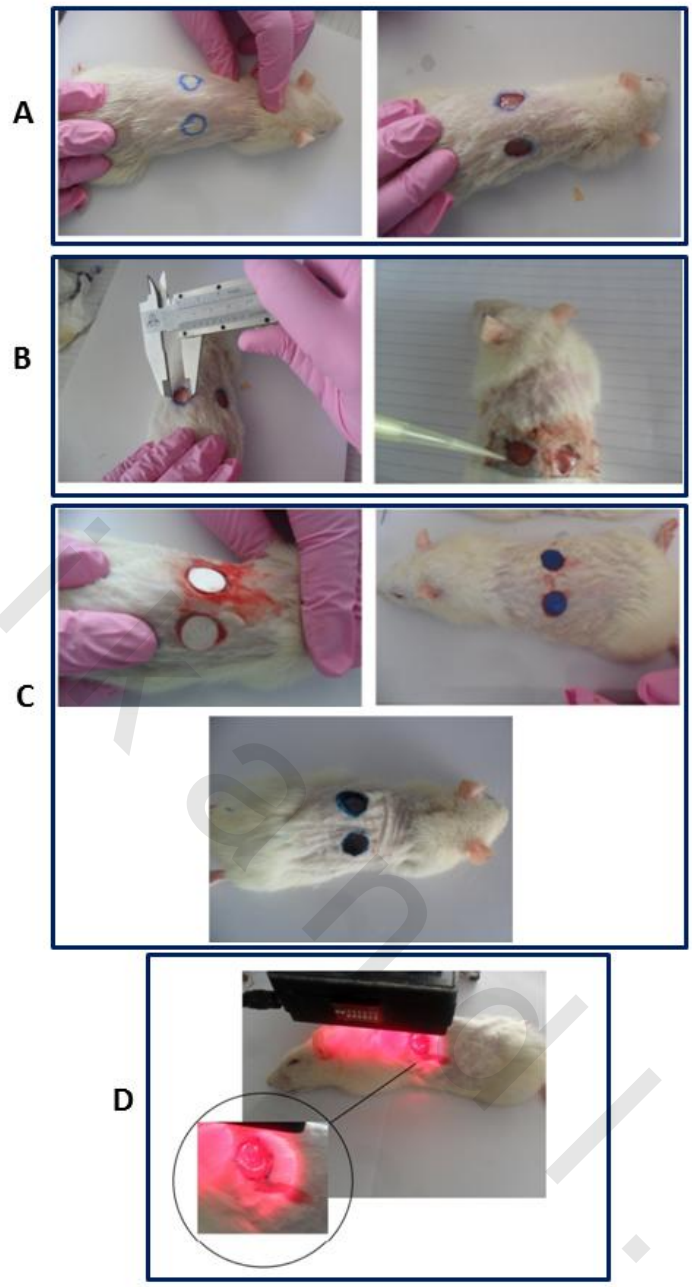

Figure 59: Steps of the surgical procedure for: A) performing two full skin thickness circular dorsal excisions in a young female *Wistar* rat followed by B) measurement of wound size using a caliper and induction of wound infection, C) application of different treatments and D) wound irradiation.

2.3.5. Study protocol

The study was designed to assess the potentials of MB-loaded PHB/PEG (3: 2) NFs as a MB-eluting wound dressing for antimicrobial photodynamic therapy using LED at 650 nm. Reduction of microbial load and healing of Sa_{st}-infected excision wounds in immunocompromized female *Wistar* rats were used as monitoring parameters. Immunosuppression was induced by cyclosporine as reported [406, 407]. The content of one Neoral® soft gelatin capsule, 100 mg/ml was diluted with 4 ml olive oil (final concentration 20 mg/ml). A daily cyclosporine dose of 20 mg/kg [408] was administered subcutaneously to all rats throughout the 15 day-study period.

A total number of 30 rats were divided into four groups and 10 subgroups, each subgroup consisting of three rats; each rat had two dorsal excision wounds. Red light emitted by LED at 650 nm and a fluence of 100 or 200 J/cm^2 was used. Treatment of the different rat groups is described in Table 14.

Untreated control rats were kept in the dark after surgery. For control rats receiving NFs treatment in the dark, a NFs membrane was placed on each excision, which was then covered with transparent Tegaderm® (3M, USA). For rats receiving treatment concomitantly with LED 650 nm illumination, a NFs membrane was placed over the wound for 30 min to allow elution of MB and to occlude the wound bed from light. The membrane was then raised away leaving the wound exposed for illumination for 25 min to provide a light fluence of 100 J/cm^2. The wound was then re-covered with the NF membrane and the animal kept in the dark. Illumination of the wound was repeated after 24 and 48 h. For MB solution groups, rats were treated with 50 µl MB solution (1.2 mg/ml) containing an amount of MB equivalent to that encapsulated in NFs. MB solution was left on the wound for 30 minutes to allow uptake by bacterial cells then illuminated at 100 J/cm^2. MB-loaded NFs or MB solution (60 µl, 0.6 mg/ml, equivalent to the amount of MB released from NFs after 24 h in presence of bacteria) were reapplied in groups 6, 7 and 10 at day 7 and 8 and illuminated at 200 J/cm^2 on both days.

After treatment, rats were returned to their cages and provided with un-restricted water supply and monitored till recovered from anesthesia. The rats remained under observation for 15 days. At the end of the experiment, rats were sacrificed with ether and the tissues from the wound site, including the whole skin thickness and surrounding skin of the individual animal were removed for histological examination and RT-PCR analysis.

Table 13: Treatments received by immunocompromized rats with infected excision wounds

Rat group	Light dose	Rat Sub-group	Code	Treatment with MB solution or NFs (light conditions)
A Dark	-	1	UT-D	Untreated
		2	MB-D	MB solution: 50 µl of 1.2 mg/ml on day 0; 60 µl of 0.6 mg/ml on days 7 and 8
		3	NFs-D	Plain NFs
		4	MB-NF-D	MB-NFs
B Light	Single 100 J/cm^2	5	UT-L	Singe irradiation at day zero
	Multiple 700 J/cm^2	6	UT-L+	Multiple irradiation (100 J/cm^2 at days 0,1 and 3; 200 J/cm^2 on days 7 and 8
	Single 100 J/cm^2	7	NFs-L	Plain NFs (100 J/cm^{2}on day 0)
		8	MB-NFs-L	MB-NFs (100 J/cm^{2}on day 0)
	Multiple 700 J/cm^2	9	MB-L+	MB solution, 50 µl of 1.2 mg/ml (100 J/cm^2) at day 0; 60 µl of 0.6 mg/ml (200 J/cm^2) with repeated application on days 7 and 8
		10	MB-NFs-L+	MB-NFs (100 J/cm^2)on day 0,1 and 3; 200 J/cm^2 with repeated application on days 7 and 8

*D = dark; L = single illumination; L+ = multiple illumination

2.3.6. Wound healing assessment

Wound healing was assessed morphologically by digital photography and wound contraction measurement, microbiologically, histologically and by gene expression analysis using reverse transcriptase-polymerase chain reaction (RT-PCR).

2.3.6.1. Wound morphological and morphometric analysis

The dimensions of wounds were measured in two perpendicular directions on days 0, 3, 7 and 15 using a caliper. The inside edge of the calipers exactly matched the edge of the wound. The percentage wound closure at each time point was derived using the formula:

$$\% \text{ Wound closure} = 1 - \left[\frac{\text{Current wound size}}{\text{Initial wound size}}\right] \text{ x } 100$$

Values were expressed as the mean ± S.D.

2.3.6.2. Microbiological assessment

The microbial load of the wound was assessed by swabbing the wound on days 1, 3, 7, 8 and 15. The swabs were cultured on mannitol salt agar plates to detect residual infection. The plates were incubated at 37ºC for 24 h. Plates were photographed and compared.

2.3.6.3. Histopathological examination

Wounds were examined histolopathologically on day 15 after sacrificing the rats. Skin tissue biopsies taken for histology were fixed in formol saline, processed and then embedded in paraffin. Sections were stained using the routine procedures Haematoxylin and Eosin (H&E) for general analysis and Masson's trichrome for assessment of collagen formation.

2.3.6.4. Reverse Transcriptase-Polymerase Chain Reaction (RT-PCR) analysis

RT-PCR analysis was performed on specimens of wound tissue taken at day 15 post-surgery to confirm the expression of selected mRNAs. These included mRNAs of two selected growth factors, namely vascular endothelial growth factor (VEGF) and platelet-derived growth factor (PDGF), an endogenous enzyme; cyclooxygenase-2 (COX-2) and a proinflammatory cytokine, tumor necrosis factor-alpha (TNF-α) using β-actin as internal control (housekeeping gene) [409].

The RT-PCR protocol used involved two steps: the RT reaction and PCR amplification. In the first step, RNA was reverse transcribed into complementary DNA (cDNA) using a reverse transcriptase. In the second step, the resulting cDNA was used as template for subsequent PCR amplification using primers specific for one or more genes. Practically, specimens were removed from the rats wound tissues on day 15 and snap-frozen [410]. Total RNA was isolated from the frozen specimens by means of TRI reagent according to the instructions of the manufacturer, treated with DNase I as a reverse transcriptase and reverse-transcribed with Omniscript Reverse Transcriptase using an oligo-dT primer as reported [411]. The optimal number of PCR cycles for each gene of interest and the control gene (β-actin) was determined by electrophoretic resolution of PCR products generated at increasing cycle numbers. For each gene, the number of cycles was set within the exponential phase. The PCR products, obtained from the exponential phase of PCR, were separated by gel electrophoresis and scanned by densitometry. To quantify relative differences in mRNA expression, densitometry values for each gene to β-actin expression at each time point were corrected and normalized by setting the highest value to 1. Primer sequences used were as follow; VEGF (F: GACCCTGGTGGACATCTTCCAGGA3- R: GGTGAGAGGTCTAG TTCCCGA), PDGF (F:CCTGTGCCATCCGCAGGAAGAGA - R: TTGGCCACCTT GACGCTGCGGTG), COX-2(F: -TGAAACCCACTCCAAACACACAG-R:5'-TCATCAGG CACAGGAGGAAG), TNF-α (F: ATGAGCACAGAAAGCATGATCCGCG- R: CCCTTCA CAGAGCAATGACTCCAAA) and β-actin (F: GGC ATC CTG ACC CTG AAG TA- R: GCC GAT AGT GAT GAC CTG). After separation of the PCR products in agarose gels and visualization with ethidium bromide, images were captured using a Kodak camera.

2.3.7. Statistical analysis

Quantitative data obtained from each experiment were subjected to statistical analysis using a one way analysis of variance test followed by a post Newman-Keuls test with $P \leq 0.05$ denoting significance. Analysis was done using GraphPad Prism 5 © software.

3. Results and discussion

In this thesis, novel photosensitizer-eluting electrospun nanofibers scaffold were presented as a wound healing matrix for APDT of localized infections. The matrix consists of electrospun PHB/PEG nanofibers loaded with MB as antimicrobial/photosensitizer. Physicochemical and photophysical characterization of the NFs indicated a biphasic *in vitro* release pattern with relatively fast initial release of MB followed by slower progressive release. MB was almost completely eluted from NFs under physiologically relevant dilution conditions. The NFs matrix protected the encapsulated MB from photodegradation. Antibacterial effect was demonstrated against two test organisms, commonly found in infected wounds, Sa_{st} and MRSA with greater activity against MRSA. Antimicrobial activity was not affected by the electrospinning process used for NFs fabrication. Photophysical studies conducted using LED at 650 nm as light source indicated that the opaque PHB/PEG NFs matrix did not allow light transmission across the NFs mat, protecting the encapsulated MB from photosensitization. However, released MB could be photoactivated with instant bactericidal effect against both test organisms. Optimized conditions for maximum antibacterial effect were 15 min dark incubation time, light fluence ranging from 100 to 200 J/cm^2 at a light intensity of 150 mW and MB concentration ranging from 50 to 100 µg/ml.

These findings suggest suitability of the MB-eluting electrospun NFs for antimicrobial photodynamic therapy of localized infected wounds. For this type of short term antimicrobial applications, it could be hypothesized that the antimicrobial effect is based on synchronization of illumination with the initial fast release phase of MB at the optimized light dose in the selected MB concentration range. Based on *in vitro* microbiological data, this treatment exerts an instant kill effect which could be maintained by the dark antibacterial effect of sustained release MB as indicated by *in vitro* release characteristics (Chapter 3).

In this chapter of the thesis, we have taken *in vitro* data further by investigating the dual ability of MB-eluting NFs/photoactivation to kill bacteria and enhance healing in an *in vivo* Sa_{st}-infected wound in a rat model, challenged by immunosuppression of the rats. The model reflects the early initial infection of a wound by a potential disease inducing organism in animals with shelved self-defense. The model also simulates clinically-relevant settings where Sa_{st} causes healing-resistant infections in immunocompromized patients. This provides broader clinical applicability as such wound treatment modalities are more needed under conditions of impaired healing either because of reduced immune response and/or virulent infective agents. Administration of Cyclosporine A to rats during wound healing at doses ranging from 5 to 17.7 mg/kg/d [406, 407, 412] was shown to induce profound immunosuppression without affecting body weight and to impair the wound healing process.

The study protocol aimed at assessing the single and combined effects of the main variables that could impact the healing of infected wounds under the conditions of the study. These are low level red light 650 nm, MB as antimicrobial photosensitizer, the plain nanofibrous matrix and the combined triple effect of light, MB and NFs.

At the outset, healing of acute cutaneous wounds is a normal intricate physiological process that proceeds through a series of coordinated cellular and cytokine-mediated events, culminating in the restoration of functional integrity of tissues [413]. The migration, infiltration, and differentiation of keratinocytes, fibroblasts, endothelial cells and macrophages lead to in an inflammatory response, cell proliferation, tissue remodeling and wound closure. This complex process is executed and regulated by an equally complex

signaling network involving numerous growth factors, cytokines and chemokines [414]. Of particular importance are the epidermal growth factor (EGF), transforming growth factor beta (TGF-b), fibroblast growth factor (FGF), vascular endothelial growth factor (VEGF), granulocyte macrophage colony stimulating factor (GM-CSF), platelet derived growth factor (PDGF), interleukin (IL) and tumor necrosis factor-alpha (TNF-α) families in addition to COX-2 as inflammation mediator in the early wound repair events that regulate re-epithelialization and angiogenesis. It should be noted that such cellular and molecular activities may be affected differently by the LED 650 nm light, MB, the nanofibrous wound healing scaffold and the immunosuppressant effect of cyclosporine A used in the study. The healing rate and quality of the experimental wounds will depend on the interplay of these factors. Thus, multiple control experiments and assessment methods were conducted to generate enough data to analyze individual effects and eventually the dual NFs/MB photoactivation effect on the healing of infected difficult-to-heal wounds.

3.1. Assessment of healing of excision wounds in immunocompromized rats without photoactivation

In this subset of experiments, group A rats (Table 13) were used to assess the wound healing and infection control effects of the MB-eluting NFs (A4-MB-NFs-D) in the absence of illumination in comparison with untreated wounds (A1-UT-D), wounds treated with MB solution (A2-MB-D) or plain NFs (A3-NF-D) as controls.

3.1.1. Morphometric and microbiological assessment

Wound morphological characteristics and % reduction in wound diameter in relation to wound infection for group A rats are shown in Figure 60a and b. Digital photographs (Figure 60a) indicated that control untreated wounds (A1-UT-D) expectedly did not close in the early healing phase with crust formation at day 7 and incomplete closure towards the end of the study. The % reduction in wound diameter attained 20% in 7 days and increased to ≈95% by day 15 (Figure 60b). Such a delay can be attributed to persistent infection of the wound throughout the study as indicated by microbiological monitoring (Figure 61a) and cyclosporine-induced suppressed immune response of the rats. Cyclosporine A was reported to impair wound healing in immunocompromized rats by inducing significant time-dependent alterations in the antioxidant enzyme profile [415] and the complicated network of interactions between connective tissue and the immune system, mainly by down-regulating the early inflammatory phase of wound healing [416]. This was evidenced by suppressed activin expression [416]. Despite immunosuppression and wound infection, no complications or deaths were observed among rats of the control group (A1-UT-D, Table 13). Resistance of rats to infection [407] and an adaptive response in antioxidant enzymes following injury under an immunocompromized situation [415] might explain the observations.

The effect of MB solution (50 µl of 1.2 mg/ml on day zero followed by 60 µl of 0.6 mg/ml at days 7 and 8, A2-MB-D in Table 13) on wound healing in the absence of illumination in comparison to untreated wounds (A1-UT-D) is shown in Figure 60 a and b. MB solution was re-instilled in the wound at days 7 and 8 to replace MB washed out by wound fluids. Data indicated that healing rates of wounds treated with MB were slightly higher compared to untreated wounds. However differences between the % reduction in wound diameter in the MB-treated groups and the control group at days 3 and 7 (Figure 60b)

were not statistically significant ($p<0.05$). Wounds did not close during the early healing phase. A crust was formed by day 7 and incomplete closure could be observed at day 15 of the study. Noteworthy, visual examination of the closing wounds revealed a jelly-like regenerated wound tissue which could be susceptible to reopening if exposed to an external force. Re-treatment of the wounds with MB solution on days 7 and 8 resulted in a slight reduction in bacterial growth (Figure 61a) despite *in vitro* antibacterial activity of MB against the Sa_{st} strain under study (Chapter 1). The relatively poor antibacterial effect of MB solution *in vivo* could be attributed to the relatively heavy infection of the wound (Initial inoculum size 10^6 CFU/ml), the non-instantaneous antibacterial effect of MB and clearance of MB solution from the wound bed under the wound hydrodynamic conditions. More complex pharmaceutical formulations such as hydrogels and delivery systems are needed to increase the contact time with the wound site and for the in-site control of MB delivery [200, 395].

Plain NFs slightly enhanced the healing process but wounds remained heavily infected throughout the study period (Figure 60a,b and 61a). The % closure data at days 3 and 7 were slightly greater than those of untreated wounds, though, the difference was not statistically significant ($p<0.05$). Wounds did not close during the early phase of healing. Crust formation and wound contraction were observed at day 7 and day 15 respectively. A main function of biodegradable NFs as wound healing scaffold implanted in incision wounds is to act as a temporary substitute to the natural ECM, guiding cell proliferation and wound healing provided that the wound infection is controlled [46]. However, we demonstrated earlier that antibiotic-eluting electrospun NFs matrices used as a protective dressing for excision wounds may also enhance wound healing by accelerating cell regeneration in the wound bed underneath [417]. On the other hand, plain non-medicated NFs are good templates for the rapid proliferation of bacteria and biofilm formation [46]. Bacterial immobilization by non-medicated dressings for the management of wounds that are in bacterial balance is considered advantageous based on the minimization of bacterial dispersion upon removal of the dressing [418, 419]. However, for wounds that are infected, bacterial sequestration may promote infection and bacterial resistance with delayed wound healing. In the present study, reduced immune response and the infection burden of the wound probably impeded the wound healing accelerating effect of NFs.

Finally, treating the wounds with MB-eluting NFs not subjected to irradiation (A4-MB-NF-D) resulted in improved wound healing with a reduction in wound diameter attaining 41% in 7 days compared to 23% for control wounds ($p<0.05$) with dark crust formation and almost complete closure at day 15 with hair growth in the wound area. Results expressed the combined cell regeneration accelerating effect of the nanofibrous matrix and antibacterial effects of the released MB. Despite fast initial release of MB, the wound infection could not rapidly subside in the early phase of wound healing probably because of the non-instantaneous MB antimicrobial effect in the dark as demonstrated in chapter 1. Greater suppression of wound infection could be observed in the later healing phase which could be attributed to the sustained release of MB from NFs and progressive wound contraction.

3.1.2. Histopathological assessment

Histological examination was performed on the last study day (15^{th} day post-surgery) for tissue specimens removed from the wounds of immunocompromized rats receiving the study treatments, MB solution, plain NFs and MB-eluting NFs. Results for histological changes in the wound bed (H & E stain) and wound margins (Masson's trichome stain) are shown in

Figure 61b, panel A and panel B respectively. Compared to normal skin (Figure 61b, A5 and B5), untreated wounds showed incomplete epithelialization and loose granulation tissue with areas of loose extra-cellular matrix lacking collagen fibers or showing immature collagen fibers in deeper layers of the wound bed (A1). At the wound margins (Figure 61b, panel B1), collagen fibers were ill-defined and showed the least staining intensity.

Wounds treated with MB solution showed more complete epithelialization. Although the wound bed showed areas of loose extra-cellular matrix, collagen fibers were more developed (Figure 61b, A2). The wound edges also showed more defined collagen fibers with deeper staining (Figure 61b, B2).

Compared to the untreated wounds, the use of plain PHB/PEG NFs matrices as wound dressings also resulted in complete epithelialization and enhanced tissue regeneration. Although, the wound center and margins showed more developed and deeper stained collagen fibers, immature collagen fibers could be observed in both regions (Figure 61b, A3 and B3).

Sections taken from wounds treated with MB-eluting NFs obviously showed more developed ECM with more mature collagen fibers and remarkable epithelialization and keratinization at the wound margins compared to all treatments (Figure 61b, A4 and B4). However, the granulation tissue was not fully resolved at the wound center. Enhanced tissue regeneration in excision wounds covered with electrospun nanofibrous matrices verified the wound healing accelerating properties of NFs wound dressings even when not implanted in the wound.

In vivo data on the use of MB-eluting PHB/PEG NFs as a wound care biomaterial, obtained for the first time in this study, indicate that these electrospun NF matrices offer promise in wound healing applications. They improved the repair of a healing-resistant infected wound in immunocompromized rats. A greater efficiency could be speculated in non-infected wounds or when used in a healthy host. The efficiency of the antimicrobial component of these matrices can be further enhanced by combining MB with an additional antimicrobial dye such as gentian violet [420]. Another enhancement approach would be photoactivation of wounds treated with these matrices under well-established conditions which is the subject of the next section.

3.2. Assessment of the healing of infected excision wounds in immunocompromized rats upon photoactivation

3.2.1. Effect of LED light 650 nm on the wound healing of infected excision wounds in immunocompromized rats

The effect of red LED light 650 nm on the healing of untreated infected wounds in immunocompromized rats was assessed using a single 100 J/cm^2 dose and repeated illuminations with total dose of 700 J/cm^2 (100 J/cm^2 on days zero, 1 and 3 and 200 J/cm^2 on days 7 and 8) in comparison with untreated wounds not exposed to the red light (A1-UT-D, Table 14).

Wound morphology (Figure 62a) indicated that single red light illumination at 650 nm slightly enhanced wound healing with the formation of a dark crust by day 7. Wounds were not completely closed at day 15. The increase in % reduction in wound diameters at 3, 7 and

15 days was not statistically significant compared to the control (A1-UT-D) wounds (Figure 62b). Single illumination did not affect wound infection throughout the study (Figure 63a).Exposure of wounds to two additional 100 J/cm^2 light doses, 1 and 3 day post-surgery significantly accelerated wound closure, reaching 22% and 46% at day 3 and 7 respectively in comparison to data for the control A1-UT-D group ($p<0.01$). The difference in % decrease in wound diameter upon multiple light exposure (B6-UT-L+) was also significant at day 7 ($p<0.05$) in comparison to single light exposure (B5-UT-L) wounds. Nonetheless, a further increase in light exposure (200 J/cm^2 at day 7 and 8 respectively) did not promote healing and incomplete closure was observed at day 15 post surgery. A slight reduction in wound diameter was even observed (89% in comparison to 91% and 94% for B5-UT-L and A1-UT-D respectively), though the reduction was not statistically significant ($p<0.05$). Multiple illumination (B6-UT-L+) had no discernible effect on the wound bacterial burden (Figure 63a). Data indicated that exposure to red light accelerated wound closure within a certain total light dose range (> 100-300 J/cm^2). A single light dose of 100 J/cm^2 proved ineffective while a total dose of 700 J/cm^2 hampered the healing process.

Histological examination of the wound beds and margins (Figure 63b) indicated that red light enhanced the integrity of the granulation tissue and deposition of collagen fibers at the wound margins, the effect being more pronounced in case of multiple irradiation. Nevertheless, all untreated wounds whether left in the dark or irradiated showed areas of loose extra-cellular matrix that lacked the presence of collagen fibers and areas with immature collagen fibers in the deep layers of granulation tissue in the wound bed.

Light-emitting diodes (LEDs) and laser generating low-level light (less than 500 mW) in the red to near-infrared (NIR) spectrum (600-1100 nm) known as low-level light therapy (LLLT) or phototherapy are reported to promote tissue repair, reduce inflammation, and relieve pain in a range of medical conditions including wound healing [421-424]. The biological effects of LEDs depend on their wavelength, dose and intensity as well as irradiation time. The basic mechanism behind the biological effects of LLLT involves absorption of red and near infrared light by chromophores contained in the protein components of the respiratory chain located in mitochondria, in particular cytochrome c oxidase [425, 426]. This causes photo-dissociation of inhibitory nitric oxide from cytochrome c oxidase leading to increased enzyme activity and increased production of ATP [427, 428]. Moreover, low-level light was shown to stimulate the expression of multiple genes related to cellular migration, proliferation, and modulate the production of growth factors and cytokines [361, 429]. Such cellular and molecular changes lead to accelerated re-epithelialization and wound healing. This explains, at least in part, the light-enhanced wound healing effect observed in this study in spite of the suppressed immune response of the animals and wound infection. As proposed by Reddy *et al* [430], light may have an optimal effect under conditions of impaired wound healing. Results obtained in this study corroborate previous preclinical phototherapy findings [431] though true value in clinical wound care needs to more investigation.

a

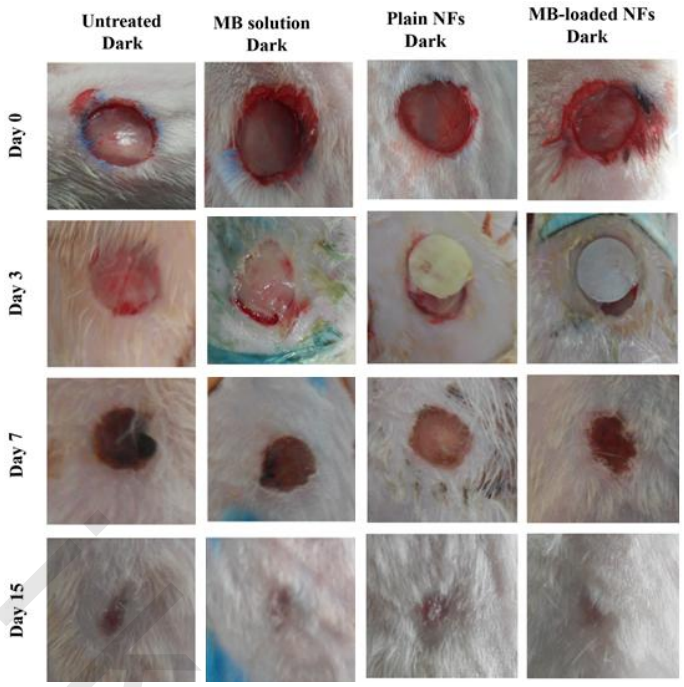

b

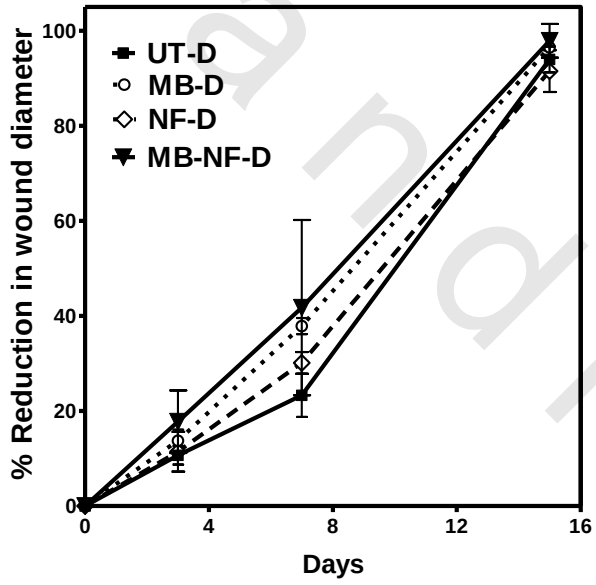

Figure 60: Effect of treatment with MB solution, plain NFs and MB-loaded NFs on a) The healing progress of excision infected wounds and b) Time-course of percentage reduction in wound diameter

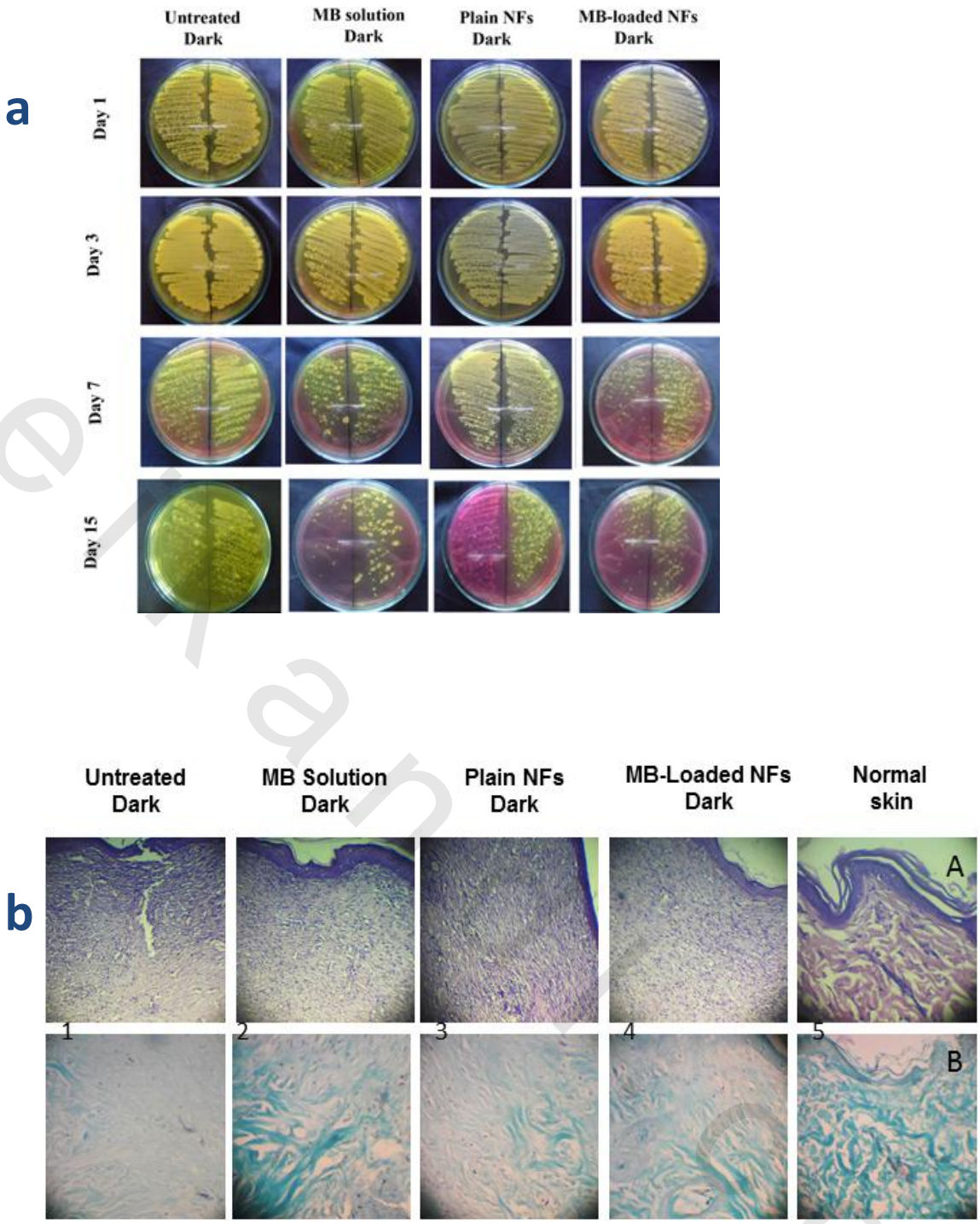

Figure 61: Effect of treatment with MB solution, plain NFs and MB-loaded on a) Bacterial contamination of the wounds over a 15 day-study period and b) Histopathological changes of excision wounds at day 15 ; wound bed using H & E staining (upper panel A) and wound edge using Masson's trichrome staining (lower panel B). Magnification: x 40

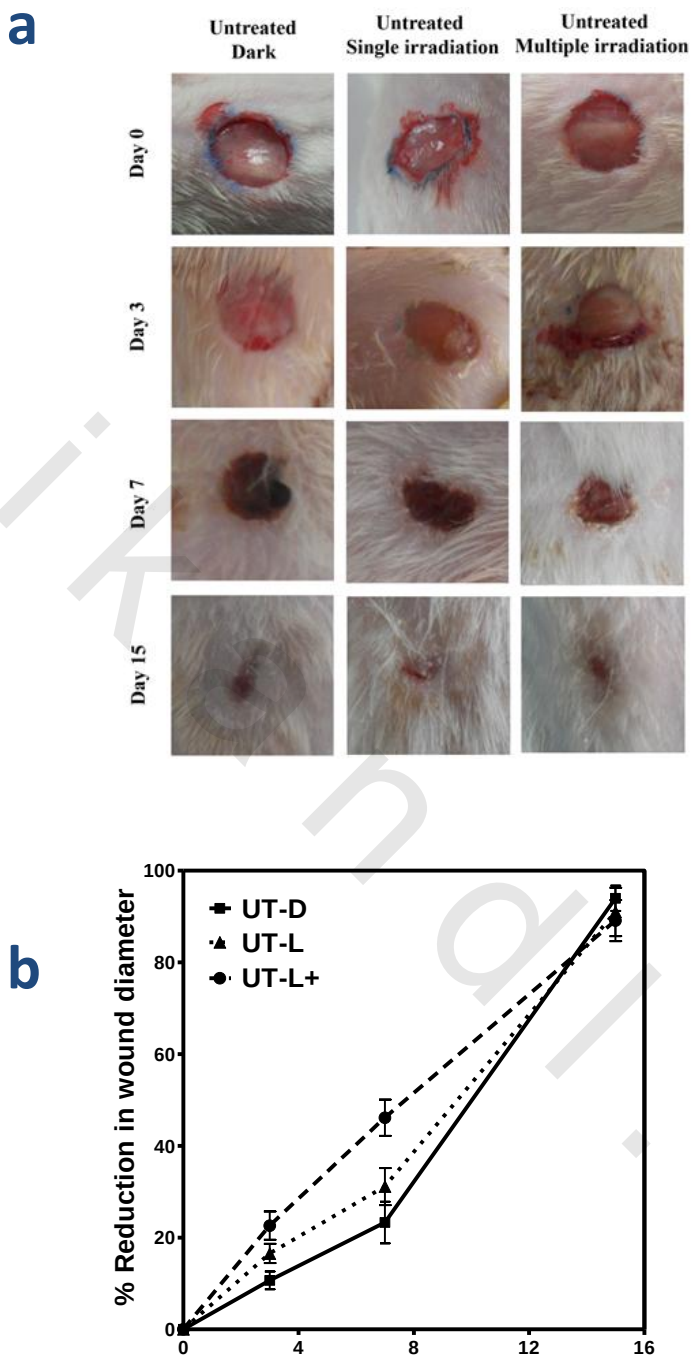

Figure 62: Effect of red LED on a) The healing progress of excision infected wounds and b) Time-course of percentage reduction in wound diameter

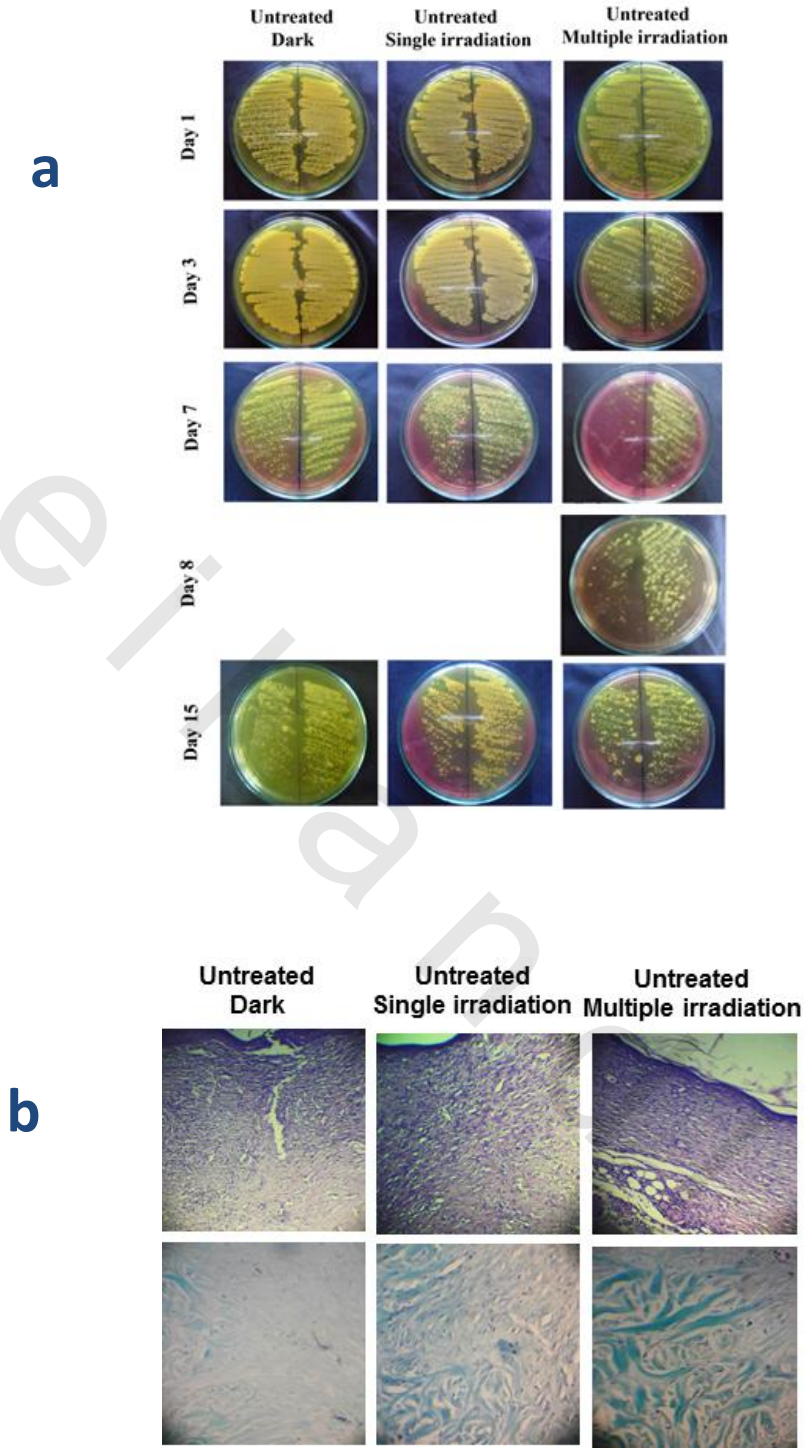

Figure 63: Effect of red LED on a) Bacterial contamination of the wounds over a 15 day-study period and b) Histopathological changes of excision wounds at day 15 ; wound bed using H & E staining (upper panel A) and wound edge using Masson's trichrome staining (lower panel B). Magnification: x 40

3.2.2. Photodynamic therapy of infected wounds in immunocompromized rats using MB-eluting NFs

In this last subset of experiments, red light (LED, 650 nm) was used for either single illumination of wounds treated with plain (B7-NFs-L) and MB-loaded NFs (B8-MB-NFs-L) or repeated illumination of MB-eluting NFs (B10-MB-NF-L+) as a dual photoactivation/NFs wound healing modality. Data for repeated illumination of MB solution were included for comparison.

Morphological characteristics of the wounds are shown in Figure 64a. Combining red light single illumination of 100 J/cm^2 at day zero and plain NFs both showing enhanced wound healing accelerating effect (Figure 62 and 60 respectively) did not significantly promote wound healing. Wounds remained open during the early healing period with the formation of a crust by day 7 (Figure 64a). The % reduction in wound diameter was 10% and 32 % at days 3 and 7 respectively (Figure 64b). Though infection did not subside throughout the study (Figure 65a), histological examination (Figure 65b) indicated epithelialization and enhanced deposition of collagen fibers at the wound margins. However, at the wound center areas, the extra-cellular matrix was loose with few immature collagen fibers. Better results were obtained by single illumination of wounds treated with MB-eluting NFs (Figure 65a). The % reduction in wound diameter attained 20% and 43% at days 3 and 7 respectively compared to 10% and 32% for plain NFs (Figure 64b) with greater reduction in bacterial load but without bacterial eradication (Figure 65a).Although a single illumination resulted in a statistically significant kill of Sa_{st} immediately after exposure and complete eradication after 24 h incubation *in vitro* (Chapter 3), this light treatment was not sufficient *in vivo* to control Sa_{st} in wounds in immunocompromized rats. Light capture by endogenous chromophores in the tissue such as oxyhaemoglobin, deoxyhaemoglobin, melanin and cytochromes was reported to reduce the amount of ROS generated by the photosensitizer [174, 175]. Despite incomplete bacterial clearance, wounds showed enhanced tissue regeneration, probably mediated by the nanofibrous wound dressing, with full epithelialization and keratinization at the wound margins with development of mature collagen fibers in the wound center (Figure 65b).

Results suggested that the dual photoactivation/NFs strategy for wound healing offers potentials in the healing of infected wounds, though the outcomes could be improved by further activation of the antimicrobial component. This was achieved by repeated illumination of wounds treated with MB-eluting NFs (B10-MB-NFs-L+). In fact, repeated illumination has been the procedure adopted for the photoactivation of photosensitizers in antimicrobial biomedical applications [195, 227]. Data for wounds treated with MB solution subjected to multiple illumination of free MB equal to that delivered by NFs (B9-MB-L+) under the study conditions were obtained for a better understanding of the healing capabilities of the dual modality. In wounds treated with MB-eluting NFs, MB delivery to the wound fluids was allowed for 30 min and the wound subjected to a single illumination at day zero with red light at 100 J/cm^2. The wound dressing was re-placed on the wound to promote healing and prevent mechanical friction and bacterial intrusion. MB progressively released from NFs at day 1 and day 3 post-surgery was photoactivated by repeated illumination of the wounds (100 J/cm^2) on both days. As a result of bacterial regrowth, wounds were treated with fresh NF dressings and illumination at higher fluence of 200 J/cm^2 on days 7 and 8. Similarly, in control wounds treated with MB solution, an amount of MB equal to that totally released from the NFs mat was instilled in the wounds on day zero and the wounds were illuminated (100 J/cm^2). Additional amounts of MB equal to the amount of MB released in 24 h were instilled in the

wounds in a solution form on days 7 and 8 and subjected to irradiation at fluence of 200 J/cm^2 on both days.

Morphological assessment of the wounds (Figure 66a) indicated superior healing of wounds subjected to the dual photoactivation/NFs treatment approach. A dark crust was formed as early as day 3 and the closed wound area at the end of the study was covered with hair. The % reduction in wound diameter was significantly greater than that of wounds treated with MB solution (Figure 66b). Wound bacteria which regrew after being subsided by photodynamic inactivation on days zero to 3 post surgery, were eradicated by multiple irradiation of wounds treated with MB-eluting NFs on days 7 and 8 (Figure 67a). A potential of photodynamic therapy is the possibility of modulating the treatment protocol on-demand. For instance, in photodynamic therapy of infected burn wounds in mice, the dose of red light had to be increased from 211 J/cm^2 to 433 J/cm^2 to eradicate regrown bacteria [178]. Histologically (Figure 67b), wound margins showed keratinization and full epithelialization. Appearance of hair follicles and remodeling of the collagen fibers at the wound margin towards normal tissue architecture was obvious, verifying morphological observations. Despite remarkable remodeling of the collagen fibers at the wound margins, the granulation tissue at the wound center was not fully resolved. Nevertheless, the significant staining intensity of the collagen fibers and their near to normal size, shape and orientation at the wound edges indicated good healing potentials of the dual photoactivation/ MB-eluting NFs as a wound healing modality.

Noteworthy, contradictory results have been reported concerning the effect of PDT on wound healing. While some studies showed a significant PDT-mediated enhancement of wound healing by promoting early formation of granulation tissue and re-epithelialization [197, 432], other studies reported no significant improvement with no healing inhibition [433] or even delayed healing [178]. Indeed, the different types of photosensitizers, light sources and energy densities used in reported studies make it difficult to compare their findings.

In the present study, morphological, morphometric, microbiological and histological data for the treatment of infected excision wounds in immunocompromized rats treated with MB-eluting electrospun nanofibers, summarized in Figure 68, suggested that these matrices offer potentials as an antimicrobial wound dressing biomaterial. Data collectively indicated that the introduction of electrospun NFs matrix as a fourth active component in APDT as a treatment modality involving light, photosensitizer and molecular oxygen greatly enhanced wound healing and infection control of the wounds, both effects being the outcome of the interplay of red light as wound healing accelerator, MB as a photosensitizer providing instant bacterial kill effect upon irradiation and antibacterial agent controlling infection post irradiation in addition to NFs as a multifunctional MB-eluting matrix with cell regeneration accelerating properties. The NFs matrix also exerted a multi-protective function by providing mechanical and bacterial protection of the healing wound bed and by protecting the encapsulated MB from photosensitization which allowed repeated illumination. Changing the NFs wound dressing kept in place during the early healing phase did not considerably affect the histological characteristics of the newly formed wound tissue, a wound healing aspect warranting further investigation. Enhanced wound healing by MB-eluting NFs-APDT implies lack of cytotoxicity of the NFs matrix, functional activity of fibroblasts, and keratinocytes in addition to effective utilization of various cells and growth factors in the wound milieu [434]. It is worth noting that the wound healing effect of NFs/ APDT components used either singly or in pairs such as light and NFs, light and photosensitizer, light and NFs, MB and NFs was inferior in all cases to the healing effect of a combination of all components.

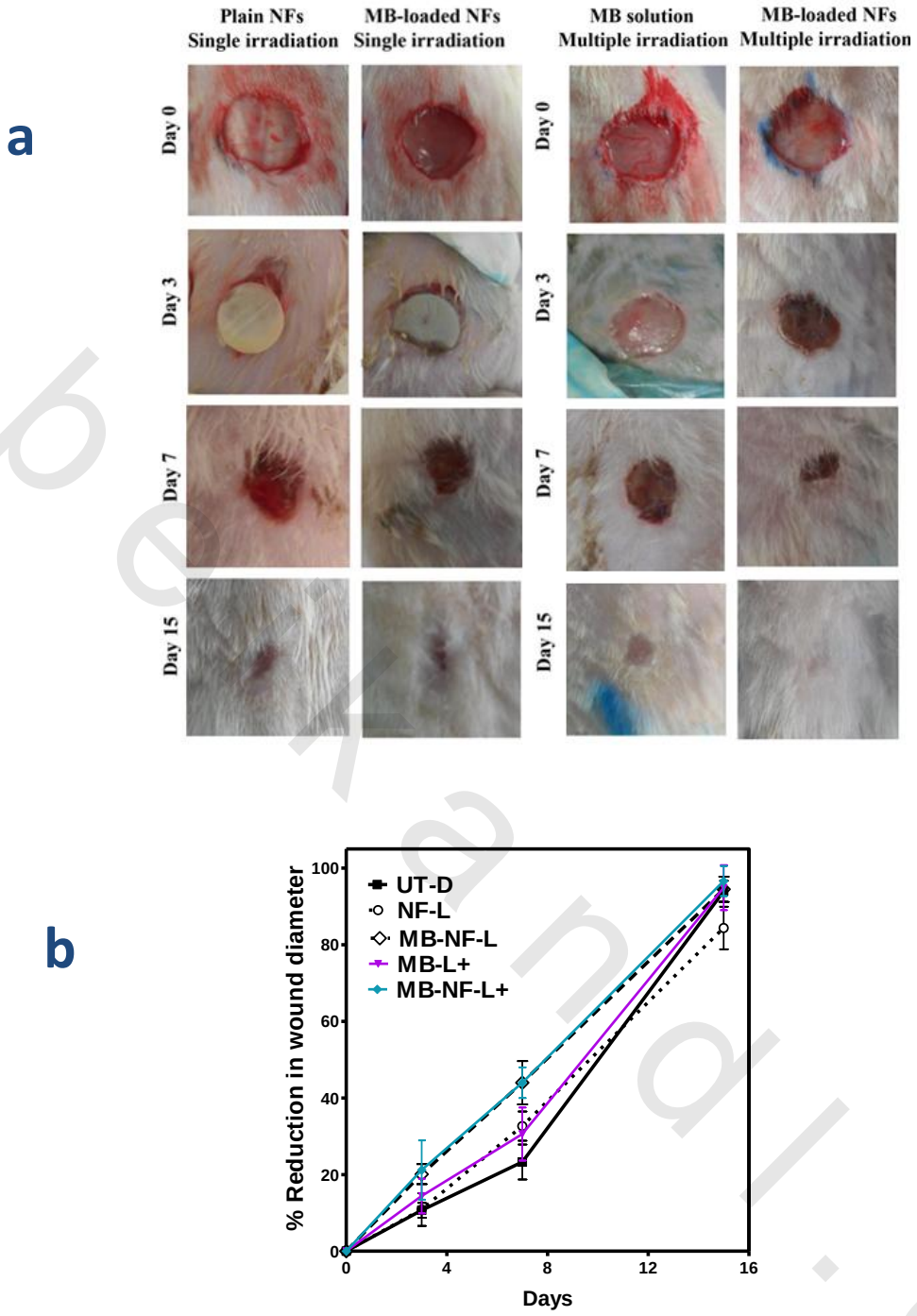

Figure 64: Effect of photoactivation/MB-eluting NFs modality on a) The healing progress of excision infected wounds and b) Time-course of percentage reduction in wound diameter

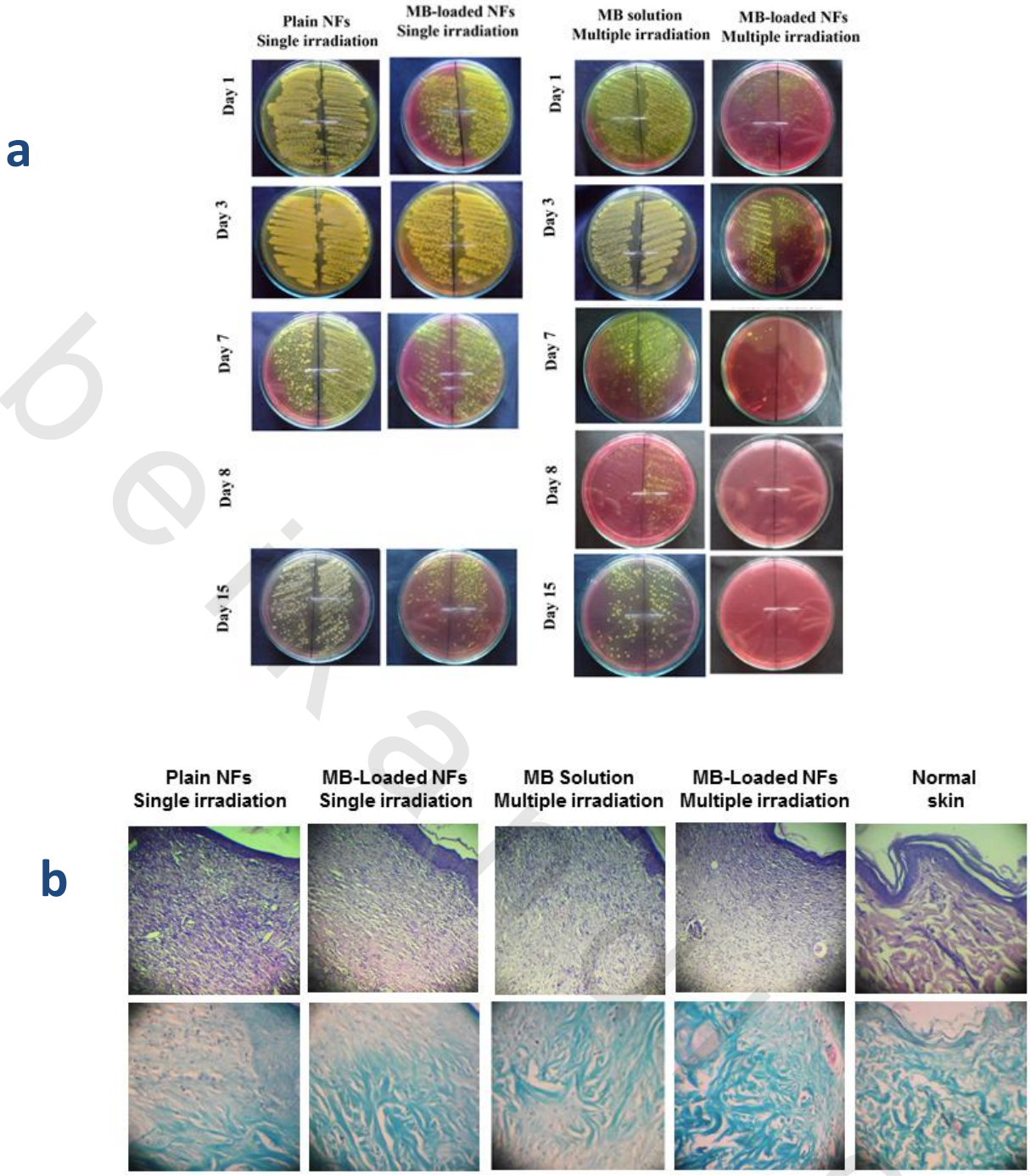

Figure 65: Effect of photoactivation/MB-eluting NFs modality on a) Bacterial contamination of the wounds over a 15 day-study period and b) Histopathological changes of excision wounds at day 15 ; wound bed using H & E staining (upper panel A) and wound edge using Masson's trichrome staining (lower panel B). Magnification: x 40

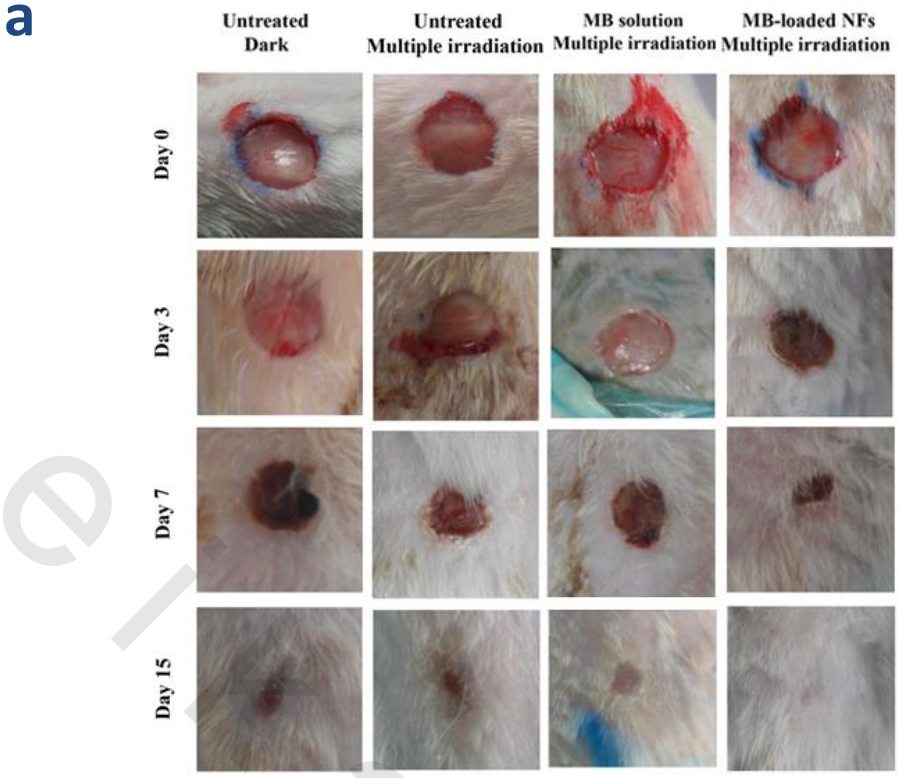

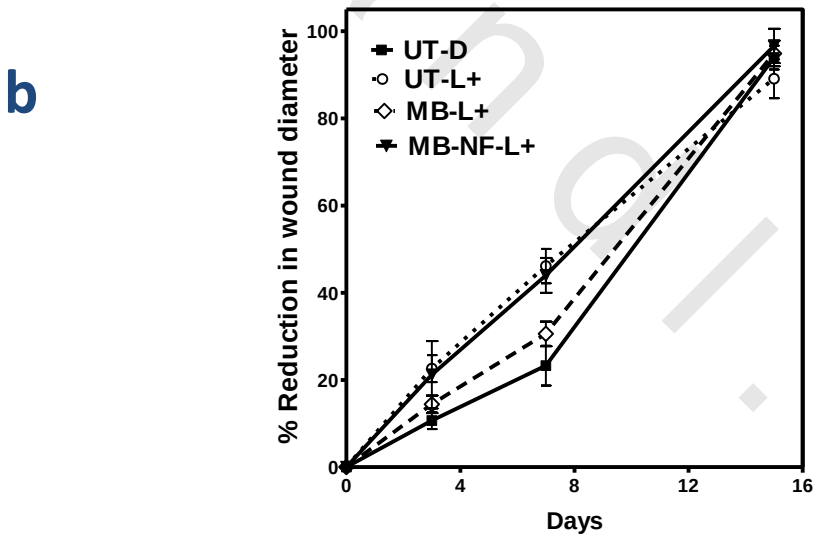

Figure 66: Summary of the effect of light, APDT and combined NFs-APDT on a) The healing progress of excision infected wounds and b) Time-course of percentage reduction in wound diameter.

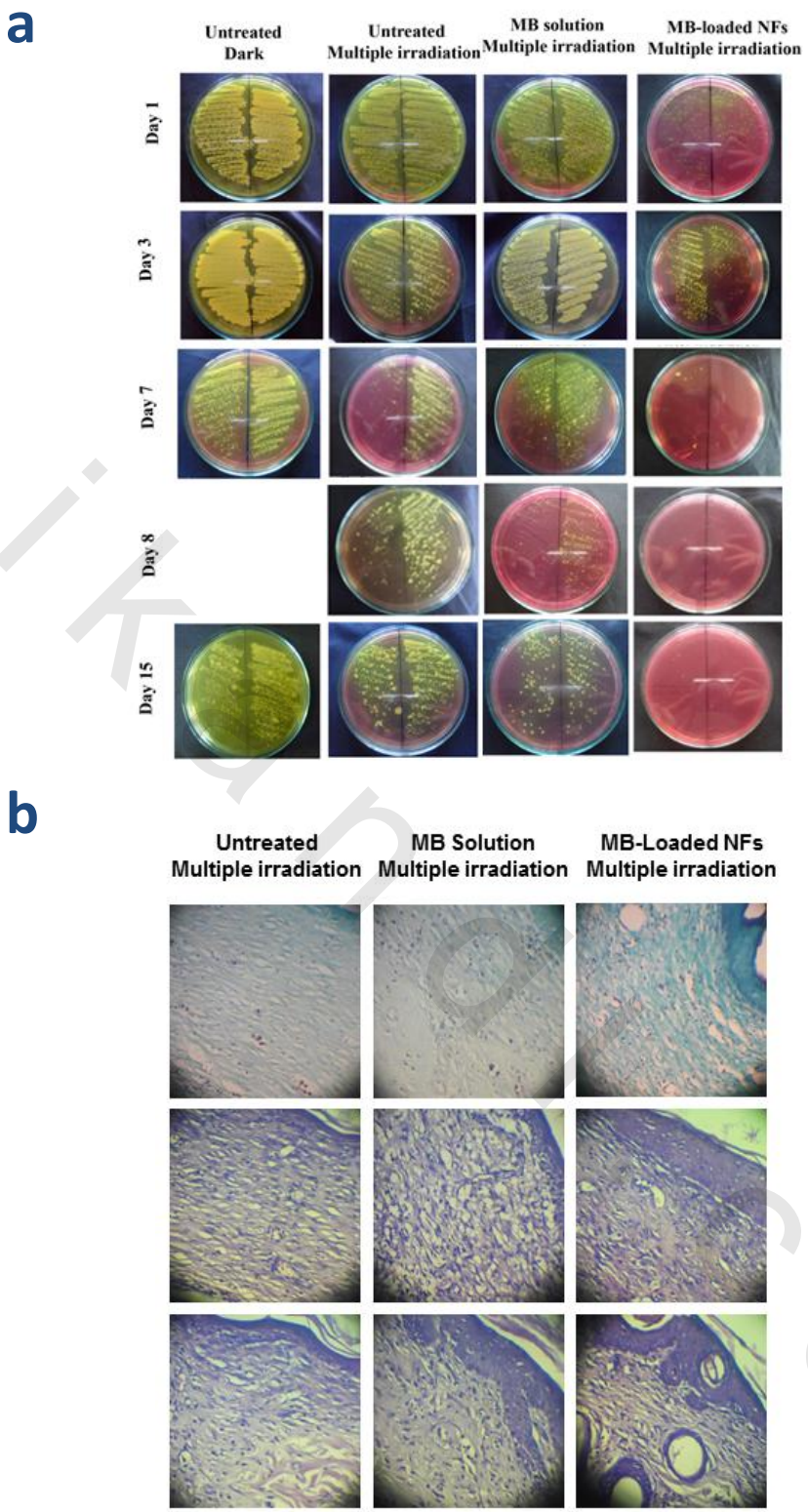

Figure 67: Summary of the effect of light, APDT and combined NFs-APDT on a) Bacterial contamination of the wounds over a 15 day-study period and b) Histopathological changes of excision wounds at day 15 showing wound bed stained with Masson's trichrome stain (upper panel A), wound bed stained with H and E stain (middle panel B) and wound edge stained with H and E stain (lower panel C) (magnification X100).

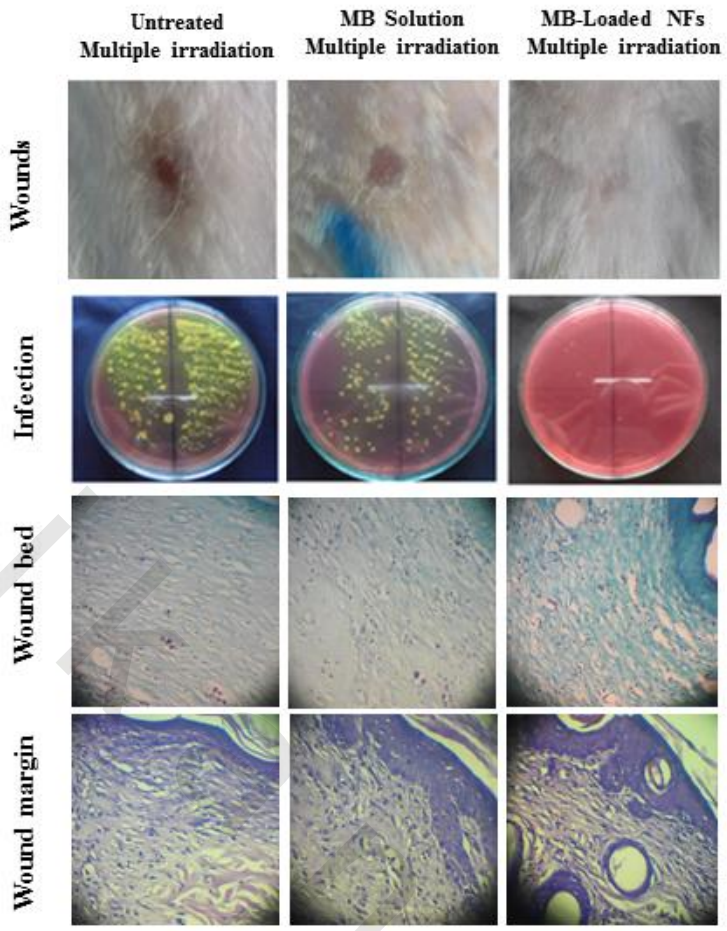

Figure 68: Summary of the morphological, microbiological and histopathological end result of treatment of infected excision wounds by light, APDT and combined NFs–APDT at day 15

3.3. RT-PCR analysis

Morphometric, microbiological and histopathological examinations assured the potentials of combined NFs-APDT as a wound dressing biomaterial for excision wounds. This combined strategy created favorable conditions in the wound that promoted controlled infection and proper healing. For a better understanding, examination of selected changes induced at the molecular level was carried out using RT-PCR. Such assessment strategies of wound-healing parameters allows to screen the efficacy of drugs, growth factors and cytokines in affecting distinct stages of the wound-healing process [8]. The effect of light therapy, APDT and combined NFs-APDT on intercellular signaling in excision wounds in rats was assessed by analyzing the gene expression of two selected growth factors: platelet-derived growth factor (PDGF) and vascular endothelial growth factor (VEGF), an endogenous enzymes, the inducible cyclooxygenase (COX-2) and a proinflammatory cytokine, tumor necrosis factor-alpha (TNF-α) using RT-PCR in comparison to the control untreated wound. Results are shown in Figure 69. The expression of mRNA of the two growth factors were generally more pronounced in wounds treated MB-NFs combined with APDT compared to the untreated control. PDGF is known to be released from platelets, keratinocytes, macrophages, and fibroblasts and is involved in inflammation, granular tissue formation, reepithelialization, and matrix formation and remodeling [414]. PDGF is also involved in fibroblast infiltration and initiation of phenotypic changes converting fibroblasts into myofibroblasts which align themselves along the borders of the ECM to facilitate wound closure [435]. VEGF is involved in the proliferation of endothelial cells ensuing angiogenesis, a process essential for the synthesis, deposition, and organization of a new extracellular matrix (ECM).

A slight increase in the expression of COX-2 mRNA in wounds treated with light, APDT and combined NFs-APDT was observed. indicating that these treatments induced an inflammatory response in the early phase of wound healing that accelerated healing [198]. The endogenous enzyme COX-2, is reported to be involved in the COX-2 pathway and other aspects of inflammation in the early wound repair events that regulate re-epithelialization and angiogenesis, impacting the outcome of repair [436, 437]. Moreover, administration of a COX-2 inhibitor was reported to delay re-epithelialization in the early phase of wound healing and inhibit angiogenesis.

PCR data also indicated the expression of TNF-α was much slighter in wounds treated with NFs-APDT compared to those treated with light or APDT. TNF-α is released by macrophages and is known to inhibit wound re-epithelialization with suppressed synthesis of ECM proteins [53]. Furthermore, non-healing wounds were reported to exhibit elevated levels of interstitial collagenases, gelatinases, and stromelysins induced by TNF-α and IL-1β [414]. Wounds treated with combined NFs-APDT showed almost disappearance of the TNF-α band, indicating enhanced wound healing and histocompatibility of PHB/PEG as a NFs polymer matrix.

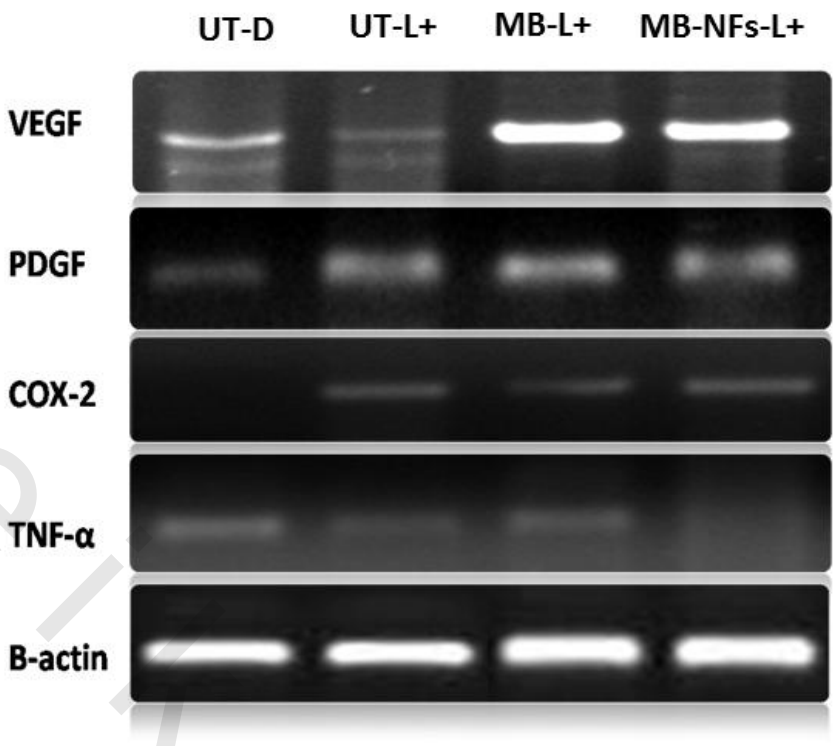

Figure 69: mRNA expression levels of VEGF, PDGF, COX-2, TNF-α and β-actin (as house-keeping gene) in excision wounds in rats treated with light therapy, APDT and combined NFs-APDT against a control of untreated infected wounds.

4. Conclusion

Multifunctional MB-eluting electrospun nanofibrous matrices are presented as a biomaterial for wound healing and antimicrobial photodynamic therapy of infected healing-resistant wounds. Without light activation, the healing properties of the matrices depends on the well-established cell regeneration guiding and accelerating effect of NFs and the antimicrobial effect of MB, not leading to antimicrobial resistance. For infected wounds, the use of MB-eluting NFs and light irradiation synchronized with the fast release phase of MB as photosensitizer provides a dual effective modality for early bacterial eradication which could be maintained by the sustained delivery of MB as antimicrobial agent into the wound bed and which allows on-demand re-illumination. The NFs matrix provides a protective barrier to the wound absorbs wound exudates and effectively contributes to the wound tissue repair. As a drug delivery system, NFs delivers MB according to a biphasic pattern allowing fast early release for photoactivation and sustained release for a longer term antibacterial effect. Moreover, the light resistant NFs matrix protects encapsulated MB from photosensitization. MB is an FDA approved inexpensive agent with an inherent bacterial cell targeting ability mediated by its positive charge and promoted by the targeting ability of the LED light which restricts cytotoxicity of singlet oxygen to the more rapidly photosensitized bacterial cells relative to host cells. From a practical point of view, the dual NFs/photoactivation wound healing modality presented is a contribution to the development of combined wound healing techniques and materials. Optimization of this dual modality would facilitate the translation these research efforts into wound care in clinical practice, helping to conserve the dwindling supply of antibiotics for effective treatment of serious systemic infections.